Structural characterization and dielectric properties of the solid solutions AgPb(Sb,Bi)S$_3$

Antonio Galdámez · Fernanda López-Vergara ·
Patricia Barahona · Victor Manríquez ·
Ricardo E. Ávila

Abstract The new solid solutions AgPbSb$_{1-x}$Bi$_x$S$_3$ were prepared by solid state reactions. The phases were characterized by powder X-ray diffractions (XRD), scanning electron microscopy, and thermal analysis. The XRD patterns of different members (x=0.5, 0.7, 0.8, and 1.0) are consistent with pure phases crystallizing in the cubic PbS-type structure. The electrical characterization was carried out using ac impedance spectroscopy and dc methods. The temperature dependence of the dc conductivity shows typical semiconductor Arrhenius behavior. The impedance measurements were performed in the frequency range of 0.1 Hz to 10 MHz and at the temperature range of 15 °C to 350 °C. The ac conductivity conforms to Jonscher's universal power law. The frequency dependence of the dielectric permittivity follows the normal dielectric material behavior, and the relaxation is thermally activated. The frequency and temperature dependences of the electrical data are found to follow Summerfield scaling formalism.

Keywords Impedance spectroscopy · Transport properties · Ceramics · Chalcogenides

A. Galdámez (✉) · F. López-Vergara · V. Manríquez
Departamento de Química, Facultad de Ciencias,
Universidad de Chile,
Casilla 653, Santiago, Chile
e-mail: agaldamez@uchile.cl

P. Barahona
Facultad de Ciencias Básicas, Universidad Católica del Maule,
Talca, Chile

R. E. Ávila
Departamento de Materiales Nucleares,
Comisión Chilena de Energía Nuclear,
Casilla 188-D, Santiago, Chile

Introduction

The family of quaternary chalcogenides phases AMM′Q$_3$ (A=Cu, Ag; M=Pb, Sn, Ge; M′=As, Sb; Q=S, Se) is being studied, recently, because of its interesting semiconducting electrical properties [1–6]. The silver and copper chalcogenide contains a number of ferroelectric phases. The AMM′Q$_3$ phases have high relative dielectric permittivity (ε_r) of the order of ~10^3–10^4, which may lead to new advances in microelectronics. Thus, AgPbSbSe$_3$ and AgPbAsSe$_3$ exhibit ε_r maximum values of 2,540 (at transitions temperature range of 100–120 K) and 55,000 (at transitions temperature range of 140–170 K), in the frequency range of 0.3 to 1 KHz, respectively [1–3]. The electrical measurement, using electronically blocking electrodes (Ag$_4$RbI$_5$) in AGeAsS$_3$, (MS)$_{1-x}$(AAsS$_2$)$_x$, and (MS)$_{1-x}$(AgSbS$_2$)$_x$ (A=Ag, Cu; M=Ge, Pb, or Sn), indicated that these phases present ionic or mixed (electronic–ionic) transport via copper or silver cations [3–5]. Impedance–frequency analyses in AgMM′S$_3$ phases indicate that when M=Sn and M′=Sb the ionic transport shifts toward higher temperature [1, 2]. When tin is substituted for lead (AgPbSbS$_3$), the conductivity rises 100 times and the peak of the permittivity lowers and shifts toward higher temperatures [1–3]. Otherwise, when M=Pb and M′=As, the phases maintain their ferroelectric behavior and the conductivity decreases in three orders of magnitude.

The crystal structure of the phase AgPbSbS$_3$ is related to the natural mineral Freieslebenite which is a superstructure of Galene (PbS) [7, 8]. This phase is a mixed (electronic–ionic) conductor with values of effective capacitance of 0.167 nF and electrical conductivity of 8.91×10^{-6} S/m (at 300 K and 10 kHz of frequency) [1, 2]. Due to these values, the frequency dependence of the dielectric permittivity and conduction via silver cations make them promising

materials for high-ohmic resistors [1–5]. In this work, we synthesize $AgPbSb_{1-x}Bi_xS_3$ solid solutions by solid state reactions and analyzed by X-ray diffraction (XRD), scanning electron microscopy with the aid of energy-dispersive X-ray analysis (SEM-EDX) and thermal analysis. The electrical properties were studied by ac impedance spectroscopy and dc methods. The purpose was to investigate the consequences of substitution of Sb^{3+} by Bi^{3+} cations in the crystalline structure and electrical properties.

Experimental details

All the chemicals in this work were used as obtained: silver powder, 99.9% purity, Aldrich; lead, 99.9% purity, Merck; antimony powder, 99.995% purity, Aldrich; bismuth powder, 99.9% purity, Merck; Sb_2S_3 powder, 99.9% purity, Merck; sulfur powder, 99.98% purity, Sigma-Aldrich. All manipulations were carried out under a dry and oxygen-free argon atmosphere. The solid solutions type $AgPbSb_{1-x}Bi_xS_3$ ($x=0$, 0.2, 0.3, 0.5, 0.7, 0.8, and 1.0) were prepared by solid state reaction in evacuated quartz ampoules and could be obtained by two ways as follows: (a) Ag, Pb, Sb_2S_3, Bi, and S were mixed in stoichiometric proportions. The reaction mixture was gradually heated to 600 °C over 12 h, kept at that temperature for 5 days, and slowly cooled to 50 °C at 12 °C/h. (b) Ag, Pb, Sb, Bi, and S were mixed in stoichiometric proportions. The reaction mixture was gradually heated to 800 °C over 18 h, kept at that temperature for 3 days, and slowly cooled to 50 °C at 12 °C/h. The reaction products are the same from either of the temperature processes. The chemical composition of the samples was determined by SEM-EDX analysis using a JEOL 5400 system equipped with an Oxford LinK ISIS microanalyzer. The XRD data were collected at room temperature using a Siemens D5000 powder diffractometer, with CuK_α radiation in the 5° to 80° (2θ) range. The lattice parameters were calculated using a CHECKCELL program [9]. Differential thermal analysis (DTA) and thermogravimetric analysis (TGA) were performed on a Rheometric Scientific STA 1500H/625 Thermal Analysis System. The DTA/TGA curves were run simultaneously on each sample from room temperature to 1000 °C, in flowing nitrogen at a heating rate of 10 °C/min. The electrical properties were studied by ac impedance spectroscopy and dc methods. The experiments were conducted in the temperature range of 12 to 350 °C in argon atmosphere. The pellets for electrical measurements were uniaxially pressed at $\sim5\times10^8$ Pa, resulting in cylindrical pellets of 7 mm in diameter and thickness of 1 to 3 mm, corresponding to an average density ~2.8 gcm^{-3}. The two opposite flat surfaces of the pellets were sputtered with gold or platinum and sandwiched between the platinum electrodes of the conductivity cell. The dc current–voltage and current–temperature were measured using a Keithley model 237 source electrometer. The current–voltage curves were verified to be linear, supporting the ohmic character of the contacts. The ac impedance–frequency measurement was carried out in argon atmosphere using a Solartron Instruments model 1260 analyzer. The frequency range was from 0.1 Hz to 10 MHz with a signal level between 25 mV and 1 V.

Results and discussion

Structural characterization and thermal stability

The XRD patterns of the $AgPbSb_{1-x}Bi_xS_3$ were fully indexed in the space group Fm-3m (Fig. 1), indicated that samples with $x=0.2$, 0.3, 0.5, and 1.0 are single phases within the detection limits of X-ray diffractions. A good agreement between observed and calculated interplanar spacing, d, was observed. The values of the cell parameters are given in Table 1. The lattice constants of the solid solutions are similar and do not obey Vegard's law. The new $AgPbSb_{1-x}Bi_xS_3$ ($x=0.2$, 0.3, and 0.5) and $AgPbBiS_3$ phases have a Galene PbS-type structure, where the cubic cationic site of the Pb is occupied randomly by Ag, Pb, Sb, and Bi atoms. However, the $AgPbSbS_3$ limit phase has a structure related to the natural mineral Freieslebenite (monoclinic, $P2_1/a$) [7, 8].

SEM micrographs of the ceramic samples are shown in Fig. 2. The pellets were sintered at 400 °C by 24 h in oxygen-free argon atmosphere, resulting in a microstructure consisting of an average grain size of ~5 μm with isolated
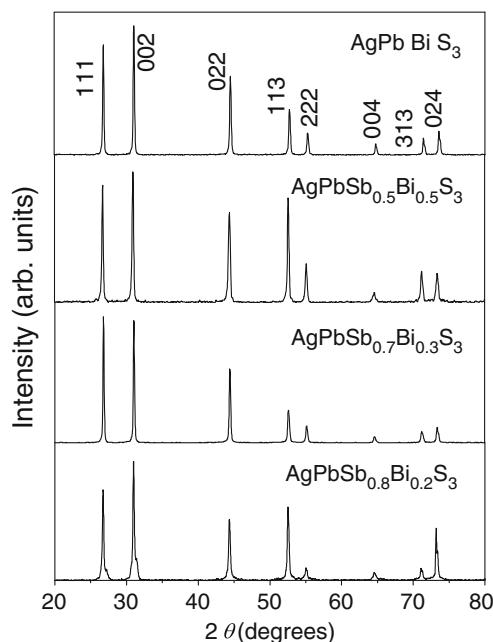
Fig. 1 XRD patterns of the $AgPbSb_{1-x}Bi_xS_3$ solid solutions

Table 1 Unit cell parameters, dc conductivity (σ_{dc}) at room temperature, and energy of activations (E_a)

| Phase	a (Å)	Volume (Å^3)	σ_{dc} (S/m)	E_a (eV)
AgPbBiS$_3$	5.75 (4)	190 (7)	2.71(4)×10^{-3}	0.52
AgPbSb$_{0.5}$Bi$_{0.5}$S$_3$	5.77 (5)	192 (9)	3.75(5)×10^{-4}	0.51
AgPbSb$_{0.7}$Bi$_{0.3}$S$_3$	5.77 (2)	192 (3)	2.14(4)×10^{-4}	0.50

regions of ~80 μm grain size. The purity, homogeneity, and stoichiometry were confirmed by backscattered SEM-EDX and XRD on the pellets of AgPbBiS$_3$, AgPbSb$_{0.5}$Bi$_{0.5}$S$_3$, AgPbSb$_{0.7}$Bi$_{0.3}$S$_3$, and AgPbSb$_{0.8}$Bi$_{0.2}$S$_3$ (Table 2). The backscattered image and EDX analysis of the pellets for electrical measurements revealed that the chemistry compositions are uniform throughout the scanned region. However, the analysis of the AgPbSb$_{0.3}$Bi$_{0.7}$S$_3$ and AgPbSb$_{0.2}$Bi$_{0.8}$S$_3$ nominal stoichiometry indicated compositional inhomogeneities. These pellets show regions rich in metallic bismuth and binary, ternary, or quaternary sulfide phases.

TGA and DTA were carried out in argon atmosphere to study the thermal stability and the possible phase transitions. Figure 3 shows the thermogravimetric analysis of AgPbSb$_{0.7}$Bi$_{0.3}$S$_3$, indicating that the decomposition occurs in two stages. The first stage, between ~400 °C and 600 °C,

produces a gradual mass loss ~1%, followed by the second stage, abrupt, ~5% mass loss process at 600 °C. Concurrently, the differential thermal signal shows several exothermic events. The first two events, with the temperature range of 400 °C to 580 °C, are understood to correspond to the gradual loss of sulfur. The event in the range of 580 °C to 680 °C can be attributed to the formation of sulfides. In addition, DTA/TGA heating/cooling was conducted in argon atmosphere, from ambient temperature up to 400 °C, resulting in stable thermal and gravimetric signals, at least, up to 350 °C. The SEM-EDX and powder XRD analysis corroborate these results. TGA and DTA of AgPbBiS$_3$, AgPbSb$_{0.5}$Bi$_{0.5}$S$_3$, and AgPbSb$_{0.8}$Bi$_{0.2}$S$_3$ solid solutions behave similarly.

Electrical measurements

The dc conductivity (σ_{dc}) of the new phases AgPbSb$_{1-x}$Bi$_x$S$_3$ is thermally activated and follows the Arrhenius behavior with activation energy of ~0.5 eV (Fig. 4, Table 1), which is comparable to that of the synthetic mineral Freieslebenite AgPbSbS$_3$ (0.481 eV). The impedance–frequency measurements of the AgPbBiS$_3$, AgPbSb$_{0.5}$Bi$_{0.5}$S$_3$, and AgPbSb$_{0.7}$Bi$_{0.3}$S$_3$ phases display a flattened arc in the Nyquist plot at room temperature (Fig. 5). The ac impedance data were analyzed using the Boukamp Equivalent Circuit program (version 2.0), assuming the parallel combination of a resistor, R, and a constant phase element, CPE. The impedance of the latter is $1/[Y_o(j\omega)^n]$, where Y_o is the admittance scale factor, j is the imaginary unit, ω is the angular frequency, and the exponent n assumes values between 0 and 1. The resistance and effective capacitance, corresponding to each semicircle, are summarized in Table 3, where R and C are ascribed to the bulk grain transport, according to the low value of C_g. The values of the χ^2 fit quality are in the range of 4.9×10^{-4} to 3.1×10^{-4}. The values of n, clearly below 1, indicate that the charge
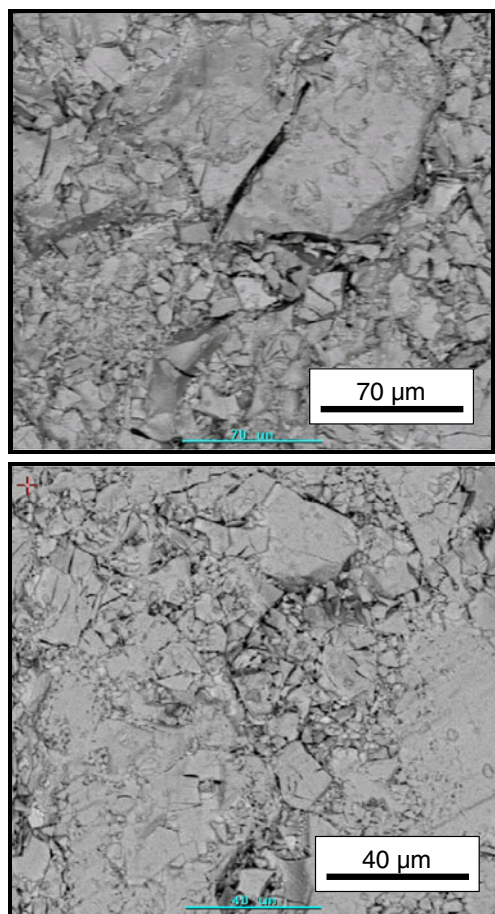

Fig. 2 Backscattered SEM micrographs of AgPbSb$_{0.5}$Bi$_{0.5}$S$_3$ (*top*) and AgPbBiS$_3$ (*bottom*) sintered at 400 °C in argon atmosphere

Table 2 Chemical composition analysis (% mass) of the AgPbSb$_{1-x}$Bi$_x$S$_3$ solid solutions

| Phases	Ag	Pb	Sb	Bi	S
AgPbSb$_{0.8}$Bi$_{0.2}$S$_3$	16.3	18.9	15.6	2.60	46.6
AgPbSb$_{0.7}$Bi$_{0.3}$S$_3$	18.4	22.2	12.5	5.00	41.9
AgPbSb$_{0.5}$Bi$_{0.5}$S$_3$	16.9	19.1	8.60	6.90	48.5
AgPbBiS$_3$	18.1	20.9	–	14.3	46.7
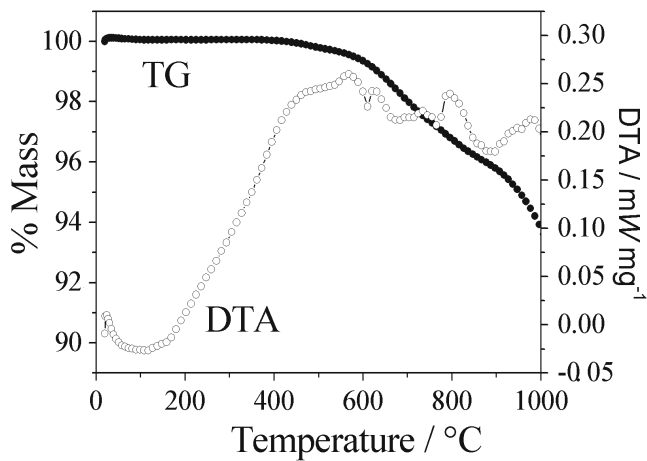
Fig. 3 Thermal analysis (DTA/TG) of $AgPbSb_{0.7}Bi_{0.3}S_3$

transport is inhomogeneous with complex network of carrier paths. The dc electrical conductivity (σ_{dc}) values are in agreement with the ac conductivity (σ_{ac}) inferred from the low-frequency trend observed in the ac impedance measurements, indicating that no other feature (arc or other) is to be suspected at lower frequencies in the Nyquist diagrams. Thus, the observed impedance is ascribed solely to bulk electronic transport, ruling out grain boundary or electrode polarization effects. The conductivity values, at room temperature, in the range of 2 to 27×10^{-4} S/m (Table 1) are an order of magnitude larger than that of $AgPbSbS_3$ (5.34×10^{-5} S/m) [1]. The dc and ac electrical conductivities, at room temperature, of the phases $AgPbBiS_3$, $AgPbSb_{0.5^-}Bi_{0.5}S_3$, and $AgPbSb_{0.7}Bi_{0.3}S_3$ show a dependence on the degree of substitution of Sb by Bi. In Table 1, the electrical conductivity is seen to increase with the values of x
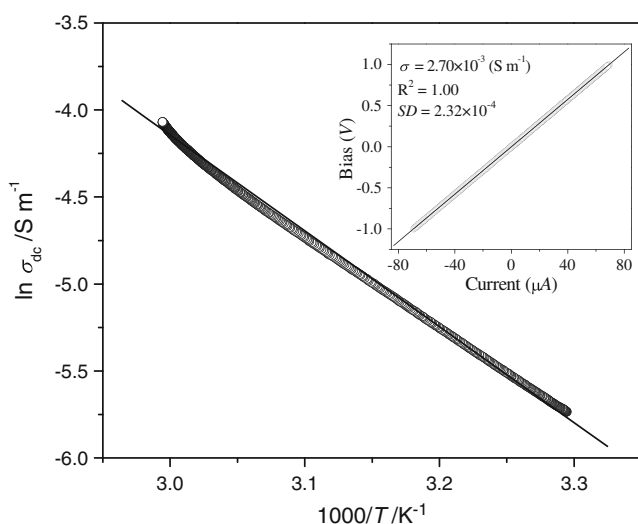
Fig. 4 The dc conductivity vs. reciprocal temperatures of $AgPbBiS_3$. The *inset* shows current–voltage curve. The *solid lines* show the linear fit to the experimental data
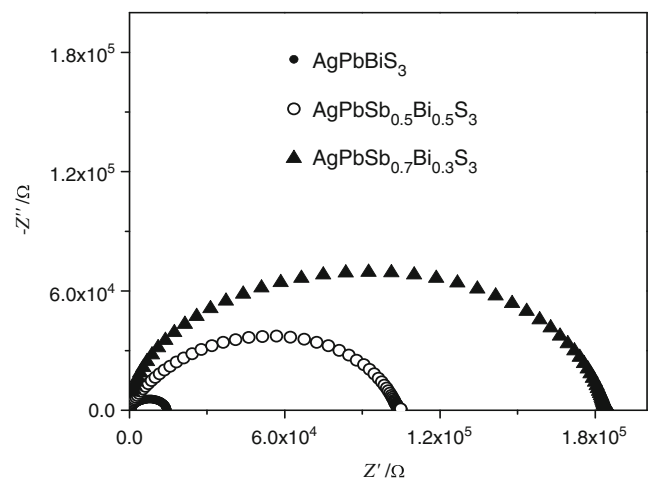
Fig. 5 Nyquist diagram at room temperature of $AgPbBiS_3$, $AgPbSb_{0.5}Bi_{0.5}S_3$, and $AgPbSb_{0.7}Bi_{0.3}S_3$

($AgPbSb_{1-x}Bi_xS_3$), and the lattice parameters remain constant upon substitution of Sb^{3+}(0.78 Å) by Bi^{3+} (1.03 Å).

The Fig. 6 shows permittivity vs. frequency plot in the temperature range of 12 °C to 350 °C (10^2–10^6 Hz frequency range). The dielectric permittivity is sharply decreasing vs. frequency, up to ~10^5 Hz. However, the dielectric permittivity remains nearly constant up to about 10^6 Hz. This behavior also has been observed in chalcogenide glasses, $Ba_3V_2O_8$ ceramic, and lithium vanadate $Li_xV_2O_5$ [10–13]. The low-frequency dispersion of the permittivity in $AgPbBiS_3$, $AgPbSb_{0.5}Bi_{0.5}S_3$, and $AgPbSb_{0.7}Bi_{0.3}S_3$ phases may be due to space charge effect arising from electrode polarization, which is produced by the mobility of ions and imperfections in the materials. In addition, the permittivity at low frequency is thermally activated, similarly as the electrical conductivity.

The ac conductivity (σ_{ac}) vs. frequency plot shows a transition, near 0.6 MHz, between the frequency-independent to frequency-dependent regions (Fig. 7). The overall frequency dependence follows Jonscher's universal power law: $\sigma_{ac} = \sigma_{dc} + A\omega^s$, where the exponent $s = (2/\pi)\tan(r)$, r being the ratio of energy lost to energy stored per cycle [14]. The values of exponent s for $AgPbSb_{1-x}Bi_xS_3$ are in the range of 1.0–1.3 and are similar to the values observed in $K_{0.5}Bi_{0.5}TiO_3$ [15]. The frequency dependence of the conductivity is interpreted as the result of changes in

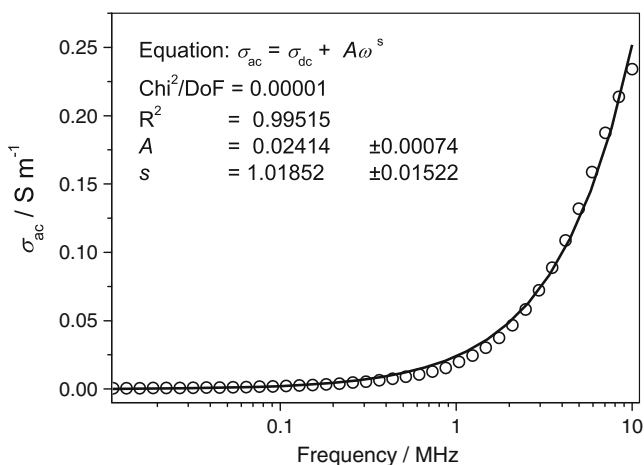Table 3 Fitting impedance parameters using the equivalent circuit at room temperature

Phase	n	R (Ω/m)	C_g (pF)
$AgPbBiS_3$	0.83 ($\pm$0.2%)	373 ($\pm$3%)	50.9 ($\pm$4.5%)
$AgPbSb_{0.5}Bi_{0.5}S_3$	0.77 ($\pm$0.5%)	2,660 ($\pm$6%)	62.2 ($\pm$7.5%)
$AgPbSb_{0.7}Bi_{0.3}S_3$	0.84 ($\pm$0.3%)	4,670 ($\pm$3%)	53.8 ($\pm$3.0%)
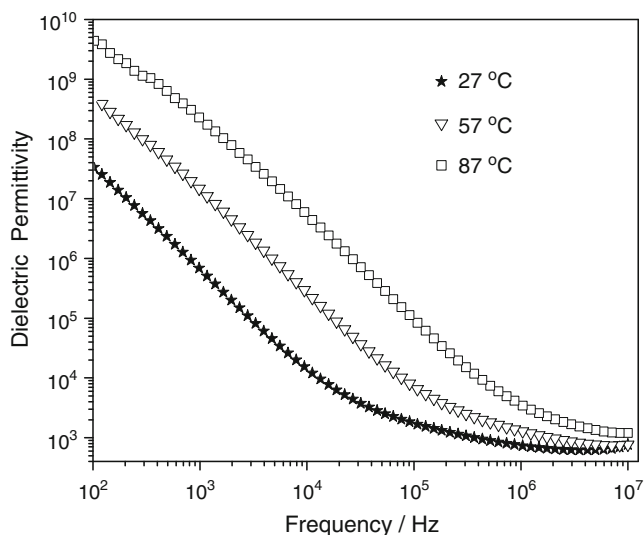
Fig. 6 Permittivity–frequency plot at different temperatures of $AgPbSb_{0.5}Bi_{0.5}S_3$

Fig. 8 Z''/Z''_{max} vs. ω/ω_{max} of the $AgPbSb_{0.7}Bi_{0.3}S_3$ phase at different temperatures. The *inset* shows M'' vs. frequency at selected temperatures of the $AgPbSb_{0.5}Bi_{0.5}S_3$

the diffusion mechanisms of ions or electronic charge carriers. Values of $s>1$ have been associated to dielectric dispersion by induced permanent dipoles or because of non-percolating charges [15–17]. In the phases $AgPbSb_{1-x}Bi_xS_3$, the dielectric dispersion may be due to either the presence of a bad site for next hop or to the coulomb repulsion between the mobile ions (for example Ag^+).

The frequency and temperature dependences of the imaginary part of the impedance (Z'') and the impedance modulus (M'') show that the relaxation is thermally activated (Fig. 8). The close overlap of the Z'' vs. frequency curves for all temperatures leads to a master curve. Alternatively, the spectral shape of the conductivity can be normalized by scaling σ_{ac} to σ_{dc} and the frequency axis by product $\sigma_{dc}T$ [18]. The Summerfield scaling procedure $\sigma_{ac}/\sigma_{dc}=F(\omega/\sigma_{dc}T)$ is shown in Fig. 9. Mariappan and
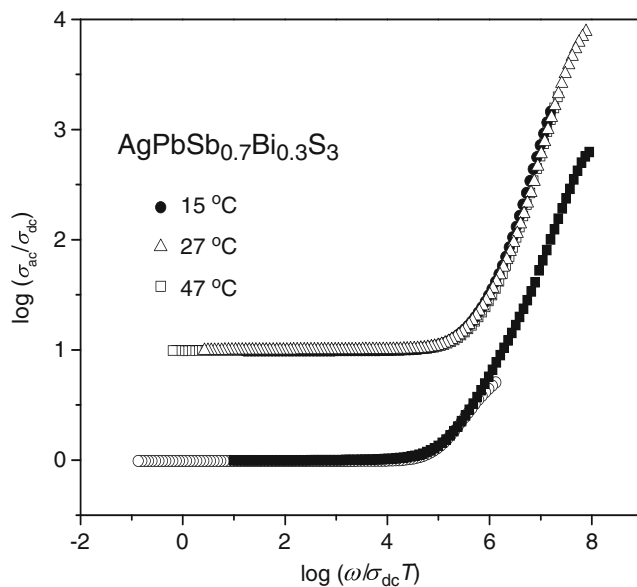
Govindaraj and Kumar and Ye have reported Summerfield scaling in Ca^{2+}-doped $SrBi_2Ta_2O_9$, $PbZr_{0.57}Ti_{0.43}O_3$, and $Na_3M_2P_3O_{12}$ orthophosphates crystalline solids [19, 20]. In addition, Basu and Maiti plotted σ_{ac}/σ_{dc} as a function of logarithmic ω/ω_{max} in doped Ba-, Sr-, and Ca-$La_2Mo_2O_9$ [21]. These are some examples in which Summerfield scaling applies to systems other than amorphous solids or ionic glasses, originally considered. The validity of the time–temperature superposition principle (TTPS) in the phases $AgPbBiS_3$, $AgPbSb_{0.5}Bi_{0.5}S_3$, and $AgPbSb_{0.7}Bi_{0.3}S_3$

Fig. 7 Non-linear fitting of ac conductivity conforming to Jonscher's universal power law

Fig. 9 Master Summerfield scaling curves of $AgPbBiS_3$ (*circle*) and $AgPbSb_{0.5}Bi_{0.5}S_3$ (*filled square*) at 27 °C. To separate the curves, the ordinate of the $AgPbSb_{0.7}Bi_{0.3}S_3$ at different temperatures is shifted by 1 unit in the log scale

implies that the temperature affects the rate of the charge transport efficiency, without introducing more than one underlying transport mechanism. In chalcogenides, such as $(MS)_{1-x}(AgSbS_2)_x$ and $AMSbS_3$ (A=Ag, Cu; M=Ge, Pb, or Sn), the mechanism of conduction is mixed, electronic and ionic (via Ag^+ or Cu^+) [3, 4]. This suggests that the electrical behavior in the $AgPbBiS_3$, $AgPbSb_{0.5}Bi_{0.5}S_3$, and $AgPbSb_{0.7}Bi_{0.3}S_3$ is due to conduction via Ag^+ ions, electronic conductions, and the compositional disorder of cation site (Ag^+, Pb^{+2}, Sb^{+3}, and Bi^{+3}) in the Galene-type PbS lattice, which creates an inhomogeneous potential environment with restricted ion movement pathways.

Conclusions

The new phases $AgPbSb_{1-x}Bi_xS_3$ were synthesized by ceramic methods at high temperature from the elements or binary sulfides. The purity, homogeneity, and stoichiometry were confirmed by SEM-EDX, and XRD indicated that samples with x=0.2, 0.3, 0.5, and 1.0 are single phases. The XRD pattern shows that the solid solutions are isostructural to Galene-type PbS. The frequency dependence of the dielectric permittivity presents normal dielectric materials behavior. The frequency dependence of ac conductivity (σ_{ac}) follows Jonscher's universal power law. The frequency dependence of the imaginary part of the impedance and the validity of the TTPS in the phases $AgPbBiS_3$, $AgPbSb_{0.5}Bi_{0.5}S_3$, and $AgPbSb_{0.7}Bi_{0.3}S_3$ imply that the relaxation is thermally activated, without introducing more than one underlying transport mechanism.

References

1. Kheifets OL, Kobelev LYa, Melnikova NV, Nugaeva LL (2007) Tech Phys 52:86–92
2. Zlokazov VB, Melnicova NV, Baranova ER, Perfiliev MV, Kobelev LYa (1992) Electrochim Acta 28:152–153
3. Baranova ER, Kobelev VL, Kobeleva OL, Melnicova NV, Zlokazov VB, Kobelev LYa, Perfiliev MV (1999) Solid State Ionics 124:255–261
4. Baranova ER, Kobelev VL, Kobeleva OL, Nugaeva LL, Zlokazov VB, Kobelev LYa (2002) Solid State Ionics 146:415–421
5. Khifets OL, Babushkin AN, Shabashova O, Melnikova NV (2007) Low Temp Phys 33:280
6. Goring YF, Melnikova NV, Baranova ER, Kobeleva OL (1997) Tech Phys Lett 23:550–552
7. Ito T, Nowacki W (1974) Z Kristallogr 139:85–102
8. Hellner E (1957) Z Kristallogr 109:284–295
9. CHECKCELL, Développed at Laboratoire des Matériaux et du Génie Physique Ecole Nationale Supérieure de Physique de Grenoble (INPG) Domaine Universitaire BP 46, 38402 Saint Martin d'Hères France, http://www.inpg.fr/LMGP or http://www.ccp14.ac.uk/tutorial/lmgp/ by Jean Laugier et Bernard Bochu
10. Stehlik S, Zima V, Wagner T, Ren J, Frumar M (2008) Solid State Ionics 179:1867–1875
11. Kahatri P, Behera B, Srinivas V, Choudhary RNO (2009) Current Applied Phys 9:515–519
12. Selvasekarapandian S, Vijayakumar M (2002) Solid State Ionics 148:329–334
13. Nobre MA, Lanfredi S (2003) Catal Today 78:529–538
14. Jonscher AK (1977) Nature 267:673–679
15. Bhaskar Rao P, Ramana EV, Bhima Sankaram T (2009) J Alloy Compd 467:293–298
16. Hirankumar G, Selvasekarapandian S, Bhuvaneswari MS, Baskaran R, Vijayakumar M (2006) J Solid State Electr 10:193–197
17. McDonald JR (1987) Impedance spectroscopy, emphasizing solid and systems. Wiley, New York
18. Summerfield S (1985) Phil Mag B52:9–22
19. Mahesh Kumar M, Ye ZG (2005) Phys Rev B 72:024104
20. Mariappan CR, Govindaraj G (2004) Phys B 353:65–74
21. Basu S, Maiti HS (2010) J Solid State Electr 14:1021–1025